PNAS RESEARCH ARTICLE | BIOPHYSICS AND COMPUTATIONAL BIOLOGY MICROBIOLOGY OPEN ACCESS

Pseudomonas aeruginosa distinguishes surfaces by stiffness using retraction of type IV pili

Matthias D. Koch[a,b,c], Matthew E. Black[a], Endao Han[c], Joshua W. Shaevitz[a,c,1], and Zemer Gitai[b,1]

Edited by David Weitz, Harvard University, Cambridge, MA; received October 23, 2021; accepted April 18, 2022

The ability of eukaryotic cells to differentiate surface stiffness is fundamental for many processes like stem cell development. Bacteria were previously known to sense the presence of surfaces, but the extent to which they could differentiate stiffnesses remained unclear. Here we establish that the human pathogen *Pseudomonas aeruginosa* actively measures surface stiffness using type IV pili (TFP). Stiffness sensing is nonlinear, as induction of the virulence factor regulator is peaked with stiffness in a physiologically important range between 0.1 kPa (similar to mucus) and 1,000 kPa (similar to cartilage). Experiments on surfaces with distinct material properties establish that stiffness is the specific biophysical parameter important for this sensing. Traction force measurements reveal that the retraction of TFP is capable of deforming even stiff substrates. We show how slow diffusion of the pilin PilA in the inner membrane yields local concentration changes at the base of TFP during extension and retraction that change with substrate stiffness. We develop a quantitative biomechanical model that explains the transcriptional response to stiffness. A competition between PilA diffusion in the inner membrane and a loss/gain of monomers during TFP extension/retraction produces substrate stiffness-dependent dynamics of the local PilA concentration. We validated this model by manipulating the ATPase activity of the TFP motors to change TFP extension and retraction velocities and PilA concentration dynamics, altering the stiffness response in a predictable manner. Our results highlight stiffness sensing as a shared behavior across biological kingdoms, revealing generalizable principles of environmental sensing across small and large cells.

Pseudomonas aeruginosa | type IV pili | stiffness sensing | surface sensing | mechanosensing

Significance

While many bacteria can sense the presence of a surface, the mechanical properties of different surfaces vary tremendously and can be as rigid as bone or as soft as mucus. We show that the pathogen *Pseudomonas aeruginosa* distinguishes surfaces by stiffness and transcriptionally tunes its virulence to surface rigidity. This connection between pathogenicity and mechanical properties of the infection site presents an interesting potential for clinical applications. The mechanism behind stiffness sensing relies on the retraction of external appendages called type IV pili that deform the surface. While this mechanism has interesting parallels to stiffness sensing in mammalian cells, our results suggest that stiffness sensing in much smaller bacterial cells relies on temporal sensing instead of spatial sensing strategies.

Bacteria thrive in many physically different environments and have developed strategies to sense distinct physical cues (1). In many bacteria, surface attachment promotes the formation of robust biofilms that offer protection from environmental insults such as fluid flow or harmful chemicals like antibiotics (2). Surface association triggers genetic programs that promote surface attachment and biofilm formation (3). Consequently, the ability to sense a surface is crucial for bacteria. Surface sensing can be mediated by membrane-associated proteins that change conformation in the presence of a surface or by obstruction of the motion of an extracellular appendage (4–9). For example, flagella are long helical appendages that generate a propulsive force enabling bacteria to swim in liquid. Attachment of either the cell body or the flagellum to the surface changes the torque on the flagellar motor, which results in stator remodeling and consequent downstream signaling (10–12). Bacterial type IV pili (TFP) represent another class of extracellular polymers that have been implicated in surface sensing. These are mostly straight filaments with a length of approximately 1 μm that drive twitching motility on surfaces through cycles of extension, unspecific binding to the surface, and retraction (13, 14). In *Caulobacter crescentus*, the bacteria sense the presence of surfaces when TFP retraction stalls, which triggers the formation of a sticky holdfast that promotes surface attachment (15).

In both of the examples above, the surface is detected in a binary fashion: The cell is either near a surface or not. While detecting the presence of a substrate is a remarkable ability on its own, the surfaces that bacteria encounter can vary tremendously in their mechanical properties and can be as rigid as bone or as soft as mucus. Sensing the extent of a surface's stiffness is an important signal for mammalian cell differentiation (16, 17). Stem cells, for example, differentiate into different types of tissue depending on substrate stiffness, and disruption of this mechanotransduction process can result in severe diseases (18, 19). Here we address the previously unanswered question of whether bacteria can also distinguish surfaces of different stiffnesses.

Stiffness is the ratio of force to deformation. Sensing substrate stiffness thus requires a cell to actively deform the substrate, measure the resulting force–deformation relationship, and transduce this information into a biochemical signal. A common

Author affiliations: [a]Lewis-Sigler Institute for Integrative Genomics, Princeton University, Princeton, NJ 08544; [b]Department of Molecular Biology, Princeton University, Princeton, NJ 08544; and [c]Joseph Henry Laboratories of Physics, Princeton University, Princeton, NJ 08544

Author contributions: M.D.K., M.E.B., E.H., J.W.S., and Z.G. designed research; M.D.K. and M.E.B. performed research; M.D.K. contributed new reagents/analytic tools; M.D.K., M.E.B., and E.H. analyzed data; and M.D.K., J.W.S., and Z.G. wrote the paper.

The authors declare no competing interest.

This article is a PNAS Direct Submission.

[1]To whom correspondence may be addressed. Email: zgitai@princeton.edu or shaevitz@princeton.edu.

This article contains supporting information online at http://www.pnas.org/lookup/suppl/doi:10.1073/pnas.2119434119/-/DCSupplemental.

Published May 13, 2022.

mechanism used by animal cells to deform the substrate is to induce contraction using focal adhesions, molecular motors, and the actin cytoskeleton. These assemblies can generate substantial forces in the nanonewton range. Information about the substrate stiffness is sensed by conformational changes in integrin complexes and transduced by phosphorylation of focal adhesion kinases (20). Bacteria are much smaller, and it has thus remained unclear whether they are capable of generating a large enough force to deform a substrate and probe its mechanical properties (21).

In the human body, commensal and pathogenic bacteria encounter a broad spectrum of mechanically different surfaces, ranging from slimy mucus in lungs to soft tissue in wounds to stiff bones. *Pseudomonas aeruginosa* is an opportunistic human pathogen that infects all of these mechanically different sites (22). TFP are important for *P. aeruginosa* virulence, and TFP-mediated surface sensing can induce multiple virulence pathways (9, 23–25). We previously showed that TFP retraction on hydrogels stimulates the production of cyclic Adenosine Monophosphate (cAMP), which activates the virulence factor regulator (Vfr), a major

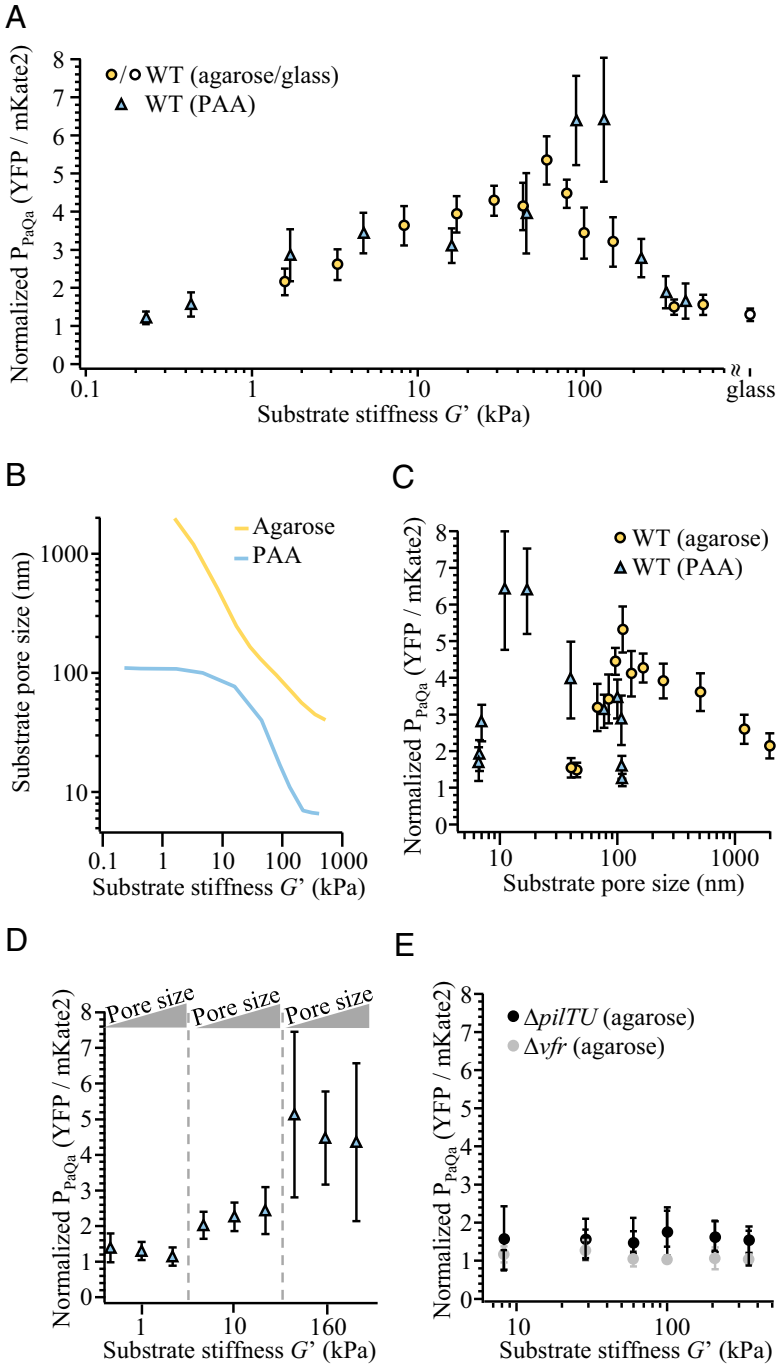

Fig. 1. *P. aeruginosa* senses substrate stiffness and the transcriptional stiffness response is peaked at intermediate stiffness. (*A*) The maximum expression of P_{PaQa} for cells on agarose and PAA hydrogels and on a glass coverslip normalized to the expression in liquid collapses as a function of substrate stiffness and is peaked between 50 and 100 kPa. (*B*) Dependence of the pore size on stiffness of agarose and PAA. The data are compiled from multiple publications (*Results* and *SI Appendix, Supplementary Methods*). (*C*) The response of P_{PaQa} on agarose and PAA hydrogels does not collapse as a function of substrate pore size. (*D*) P_{PaQa} response for PAA gels of different pore size but identical stiffness. (*E*) The P_{PaQa} responses of the retraction-deficient mutant Δ*pilTU* and a mutant lacking the transcriptional regulator Vfr (Δ*vfr*). (*A* and *C–E*) Each data point is the median of at least three biological replicates and eight technical replicates each. Error bars are the IQR of the distribution (*SI Appendix*, Fig. S1).

transcriptional regulator for more than 100 virulence-related genes including the *PaQa* operon (26).

Here we show that *PaQa* expression changes on gels with increasing agarose concentration in a complex fashion that is peaked (nonmonotonic). This behavior could reflect the sensing of substrate stiffness or a decrease in hydrogel pore size. To differentiate these possibilities, we use hydrogels of different pore sizes but similar stiffnesses and show that *PaQa* expression is specifically driven by surface stiffness. To address the molecular basis of surface stiffness, we demonstrate that TFP are capable of producing contractile forces that substantially deform surfaces. Furthermore, we find that TFP monomers (PilA) diffuse slowly in the membrane, which causes the local concentration of PilA at the TFP base to change during TFP extension–retraction in a surface-dependent manner. Informed by these results, we propose a quantitative model in which temporal changes in local PilA concentrations during TFP extension and retraction are used to measure the stiffness of a surface. Finally, we provide experimental support for this model by demonstrating that it accurately predicts how different mutants affecting PilA dynamics also affect stiffness sensing.

Results

P. aeruginosa Vfr Activity Depends on Substrate Stiffness and Is Peaked at Intermediate Rigidities. To investigate the extent to which *P. aeruginosa* can differentiate surfaces, we assessed responses of the previously characterized *PaQa* reporter of Vfr activity to a wide range of agarose concentrations. To measure the activity of the *PaQa* promoter (refered to as P_{PaQa} response), we recorded individual fluorescence time-lapse movies of *P. aeruginosa* cells growing on a variety of different gels. First, cells were grown as a liquid culture to the early log phase (optical density OD600 = 0.1), and then a 1 μL droplet of cell suspension was added to a hydrogel. Excess liquid on the surface was allowed to dry on the hydrogel, and then the gel was added to a glass-bottom Petri dish. This confined the cells between the hydrogel and the coverslip to increase substrate interaction. Notably, TFP unspecifically bind to most substrates as evident by TFP-dependent twitching motility, e.g., on agarose gels, or optical tweezers and atomic force microscopy (AFM) experiments using plastic beads or metal cantilevers (14). We then analyzed the increase in P_{PaQa} fluorescence compared to the constitutive fluorescence of the *rpoD* house keeping gene P_{rpoD} over time, where the zero time point represents the P_{PaQa} expression in liquid. The expression of P_{PaQa}::*yfp* in liquid does not change over time (26) but increases and is maximal after approximately three hours on a gel (*SI Appendix*, Fig. 1 *A–C*). Consequently, we analyzed the median and interquartile range (IQR) of the distributions of the relative fluorescence values P_{PaQa}/P_{rpoD} (YFP/mKate2) at $t = 0$ (liquid) and the maximum response for each repeat at approximately $t = 3$ h. The medians of the ratios of these values represent the up-regulation as a response to the hydrogel compared to the expression in liquid (*SI Appendix*, Fig. 1*D*).

We found that *PaQa* induction increased up to a concentration of 1.5% agarose but then decreased at higher concentrations (Fig. 1*A*). The surprising "peaked" nature of this response could result from sensing increasing stiffness or decreasing pore size for agarose gels with increasing concentration, and it is even possible that the increasing and decreasing response regimes have different dependencies on these two key parameters. To address this question, we utilized two chemically different stiffness-tunable hydrogels: polyacrylamide (PAA) and agarose. By changing the concentration of the polymer acrylamide and its cross-linker bisacrylamide, the stiffness of PAA gels can be adjusted between 0.1 kPa and 500 kPa (27). Similarly, by adjusting the concentration of agarose, the stiffness of agarose gels can be adjusted between 1 kPa and 1,000 kPa (28). As shown in Fig. 1*B* and detailed in *SI Appendix, Supplementary Methods*, the pore size of both gel types differs significantly (29–32). This difference in pore size and stiffness allows us to disentangle whether the *PaQa* response can be explained by surface stiffness or pore size. We measured the P_{PaQa} response to a variety of these hydrogels and plotted the results separately as a function of pore size and a function of stiffness (Fig. 1 *C* and *D*). If the P_{PaQa} response is a result of the changes in pore size, then we expect the P_{PaQa} response data for agarose and PAA to collapse onto each other as a function of pore size, but not as a function of stiffness. In contrast, if the P_{PaQa} response is a result of a change in stiffness, then the response for agarose and PAA should collapse as a function of stiffness, but not as a function of pore size.

We first compared the P_{PaQa} response on PAA to that on agarose as a function of substrate stiffness (Fig. 1*A*). The measured P_{PaQa} responses for both gel types collapsed almost perfectly onto each other over a 4-order-of-magnitude range in stiffness, suggesting that the P_{PaQa} response to a hydrogel is a result of a change in stiffness. This response was peaked at an intermediate stiffness of 50 to 100 kPa. To test whether this high stiffness decrease is a possible hidden effect of ever-decreasing pore sizes, we next plotted the same P_{PaQa} response data as a function of pore size (Fig. 1*C*). Here, the responses for both gel types did not collapse onto each other. In fact, both responses did not overlap at all and the response to PAA peaked below the smallest pore size of all agarose gels, supporting the idea that the observed high stiffness decrease of P_{PaQa} is not a hidden effect of a small pore size but is rather a response to high substrate stiffness. In contrast, the doubling time of individual cells during the P_{PaQa} time-lapse experiments depended on pore size but not stiffness (*SI Appendix*, Fig. 3). As a further control, we varied the concentration of acrylamide to cross-linker to make gels with the same stiffness but different pore sizes following the method described by Wen et al. (33). Specifically, we made three gels of different pore size for each stiffness of $G^* = 1$ kPa, 10 kPa, and 160 kPa. As expected, the P_{PaQa} response changed with gel stiffness but not pore size (Fig. 1*D*). We also confirmed that the lack of *PaQa* induction at high stiffness is not due to a general defect in gene induction; both P_{PaQa}::*yfp* and P_{rpoD}::*mKate2* fluorescence does not decrease on these gels over time while cells grow and divide, demonstrating that both fluorophores are continuously being made (*SI Appendix*, Fig. 4 *A–F*). In addition, we also confirmed that independent promoters such as *pBad* and *pTet* are substrate stiffness–independent by including arabinose or tetracycline in the hydrogels (*SI Appendix*, Fig. 4*G*). Finally, our findings predicted that *PaQa* should be poorly induced by highly stiff surfaces, and we confirmed that *PaQa* was not significantly induced upon association with glass (Fig. 1*A*). We conclude that the substrate-dependent P_{PaQa} response is a response to stiffness and that this response is peaked at intermediate substrate stiffness.

We previously demonstrated that the P_{PaQa} surface response depends on TFP retraction, and we sought to determine whether this is also true for stiffness sensing. As shown in Fig. 1*E*, the P_{PaQa} response of a Δ*pilTU* mutant that still makes TFP but is unable to retract the TFP is independent of surface stiffness. Similarly, disrupting the sensing pathway by deleting the Vfr also abolishes stiffness sensing.

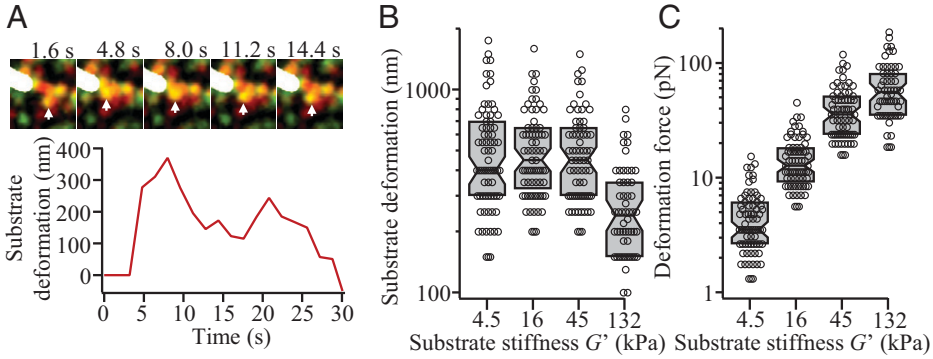

Fig. 2. Forceful TFP retraction deforms and force probes stiff substrates. (*A*) TFM example of a substrate deformation (white arrow) caused by pilus retraction toward the cell on a stiff 132 kPa PAA gel. The substrate deformation was obtained by particle tracking (Movie S5). (*B*) Substrate deformation of individual pilus retraction events on substrates with different stiffness obtained by particle tracking ($n > 58$ each). (*C*) Deformation force for the individual deformations in *B* as a function of substrate stiffness ($n > 56$ each). (*B* and *C*) Gray boxes are the median and 25/75% quartiles.

TFP Retraction Forces Deform Substrates across the Stiffness Range Sensed by *P. aeruginosa*. How can individual bacterial cells sense the stiffness of their surrounding substrate? Stiffness is the degree to which a material resists deformation. The stiffness of a spring, for example, is given by the spring constant $k = F/\Delta x$ and is a measure for the spring's resistance to an applied force F that yields a stretch Δx. Similarly, the 1-dimensional deformation Δx by the force F of the surface layer of a gel with the shear modulus G' is given by $F = \frac{4}{3}\pi G' R\Delta x$, where R is the radius of the spot to which the force is applied (*SI Appendix*, *Supplementary Methods* and Fig. S5*A*). In other words, any stiffness-sensing mechanism must be able to apply a force sufficient to deform the surface and measure the resulting deformation. Since the stiffness-dependent P_{PaQa} response relies on PilTU-dependent TFP retraction (Fig. 1*E*), we hypothesized that substrate stiffness could be sensed by a molecular sensor that measures the force and/or deformation of the substrate when gel-attached TFP retract.

To directly determine whether *P. aeruginosa* PAO1 deforms substrates, we next used traction–force microscopy (TFM) to see whether TFP retraction causes local substrate deformation. In TFM, small 40 nm diameter fluorescence beads are embedded densely into the hydrogel substrate and imaged in a time-lapse experiment (34). Substrate deformations become apparent because gel-bound beads get displaced together with the substrate (Fig. 2*A*). TFP caused substrate deformations in front of the pole of individual cells on soft 4.5 kPa gels, intermediate 16 kPa and 45 kPa gels, and stiff 132 kPa gels (Movies S1–S4). We used single-particle tracking to measure the surface deformation caused by individual cells for the different substrates (*SI Appendix*, *Supplementary Methods*). This analysis shows that even for the stiff 132 kPa substrates, TFP can still cause measurable deformation (Fig. 2*B* and Movie S5). In the example shown in Fig. 2*A*, pilus retraction stalled slowly over 4 s and deformed the gel by ∼350 nm before slowly relaxing back. Quantifying substrate deformations for a range of gel stiffnesses shows that gel deformation is maximal for soft substrates and declines only for very stiff substrates (Fig. 2*B*).

Our data also enabled us to determine the size of the TFP region that pulls on the surrounding gel. The fact that substrate deformations are constant for substrate stiffnesses < 100 kPA suggests that deformations are limited by TFP length, because TFP fully retract. Only on stiff gels are surface deformations ae not limited by TFP length but by TFP retraction force. Consequently, the deformation force for stiff 132 kPa gels equals the maximum TFP stall force. Thus, setting the median deformation force F_s equal to the stall force we obtain the TFP attachment spot size $R = \frac{3}{4\pi G' \Delta x F_s} = 0.84$ nm. Here, the deformation force is the maximum force that TFP generate during retraction. Since this force has been shown to vary between different strains, we estimate the maximum retraction force of *P. aeruginosa* PAO1 to be 55 pN using optical tweezers (see *SI Appendix*, Fig. 6) (35–38). Interestingly, the small size of this derived contact region suggests that TFP are unlikely to interact with gels along the length of the pilus but rather attach via a small contact area, as one might expect if binding occurred at the TFP tip. Scaling the substrate deformations in this manner shows that the traction force applied to deform the substrate increases monotonically with substrate stiffness (Fig. 2*C*). Together, these results show that TFP can deform even stiff substrates, in support of the hypothesis that TFP retraction causes substrate deformation, which can be sensed by a molecular stiffness-sensing mechanism.

The Local Concentration of PilA at the Pilus Base Changes during TFP Extension–Retraction in a Surface-Dependent Manner. The loss of stiffness sensing in TFP retraction mutants indicates that the response to stiffness relies on the retraction of TFP. We therefore imaged TFP retraction on different surface stiffnesses by fluorescently labeling the PilA TFP subunit using a cysteine–maleimide labeling technique (39). PilA can exist in two stable forms: monomers that reside in the inner membrane and polymers that form TFP. TFP extension motors remove PilA from the membrane to polymerize them into TFP at the base of the pilus, while retraction motors depolymerize TFP to release PilA monomers into the inner membrane at the site of the pilus base. Interestingly, we observed that the local concentration of PilA at the base of dynamic TFP changes during TFP extension and retraction. We first measured the local PilA fluorescence intensity at the base of extending TFP that are not in surface contact (Fig. 3 *A* and *B*). For example, the pilus shown in Fig. 3*A* extended for approximately 13 s to a length of approximately 5 μm. During this time, the fluorescence intensity at the pilus base decreased by approximately 20%. Immediately afterward, the pilus retracted completely back into the cell for approximately 7 s and the fluorescence intensity at the base simultaneously increased. Interestingly, upon retraction the local PilA intensity at the pilus base initially increased to higher levels than before pilus extension, only to decrease slowly again to initial levels several seconds after the pilus was fully retracted.

We next examined the local changes in PilA levels at the pilus base in TFP attached to a stiff substrate. We thus imaged local PilA concentrations at the base of TFP bound to a stiff 4.0% (350 kPa) agarose gel (Fig. 3 *C* and *D*). Here, the pilus

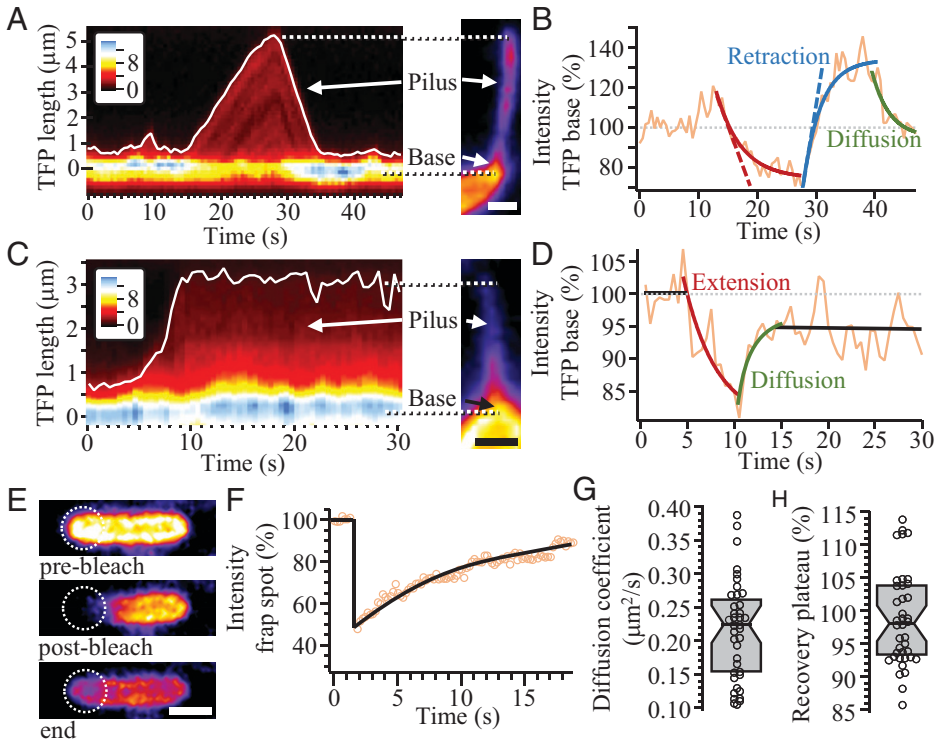

Fig. 3. The local concentration of PilA at the base of dynamic TFP changes during TFP extension-retraction in a substrate dependent manner. (*A*) Kymograph of the PilA-Alexa488 fluorescence intensity along the dynamic pilus without surface attachment shown on the right (Scale bar, 1 μm). *Inset*: fluorescence intensity, arbitrary units (a.u.). (*B*) Analysis of the fluorescence intensity from (*A*) at the pilus base indicative of the concentration of PilA. Thick/dashed red, blue, and green lines are exponential/linear fits. (*C*) Kymograph of the PilA-Alexa488 fluorescence intensity along the dynamic pilus attached to a 4.0% agarose gel shown on the right (Scale bar, 1 μm). *Inset*: fluorescence intensity (a.u.). (*D*) Analysis of the fluorescence intensity from (*C*) at the TFP base indicative of the concentration of PilA. Thick red and green lines are exponential fits. (*E*) Three frames of a FRAP experiment of Alexa488-labeled PilA. The dashed circle illustrates the photobleaching spot (Scale bar, 1 μm). (*F*) Fluorescence intensity at the photobleaching spot in (*E*) over time, corrected for overall bleaching (*SI Appendix, Supplementary Methods*). The thick black line for t > 1.5 s is an exponential fit. (*G*) Diffusion coefficient obtained by individual FRAP experiments ($n = 39$). (*H*) Recovery plateau of postbleach fluorescence at the bleach spot compared to before bleaching, indicative of the immobile fraction of PilA, obtained by individual FRAP experiments ($n = 39$). (*G* and *H*) Gray boxes are the median and 25/75% quartiles.

extended to a 3 μm length and retraction stalled immediately as the tip adhered to the gel, indicated by a straining of the pilus and a slight movement of the cell toward the TFP tip (Movie S6). As expected, the fluorescence intensity at the pilus base increased slowly upon stalling but did not overshoot the initial intensity level compared to the unbound pili (Fig. 3 *A* and *B*). Once equilibrated by diffusion ($t > 15$ s), the fluorescence level remained lower than the initial level prior to pilus extension. These findings are consistent with a model in which surface binding slows TFP retraction, thereby reducing the rate and extent to which PilA is recycled back into the membrane.

Diffusion of PilA in the Inner Membrane Is Slow Compared to TFP Extension and Retraction. Our findings that PilA levels change at the pilus base during TFP extension and retraction surprised us because the rapid diffusion of proteins typically equilibrates local fluctuations in protein so quickly that they cannot be observed by traditional microscopy. However, PilA monomers are membrane-associated, and membrane-associated proteins diffuse slower than cytoplasmic proteins. If the rate at which PilA monomers diffuse in the inner membrane is slower than the rate of monomer removal or addition due to TFP extension or retraction, then the local depletion of PilA monomers by TFP assembly could overwhelm diffusion, leading to the observed transient decrease in PilA at the base. Likewise, during retraction, TFP would be locally inserted into the membrane faster than they diffuse away, leading to a transient increase in PilA at the base.

To test this hypothesis, we used fluorescence recovery after photobleaching (FRAP) to measure the diffusion coefficient of PilA in the inner membrane. We photobleached fluorescent PilA at one TFP-free pole of the cell with a focused laser for less than 1 s and measured the dynamics of fluorescence recovery due to the diffusion of unbleached monomers from the rest of the cell (*SI Appendix, Supplementary Methods* and Fig. 3 *E* and *F*) (40). This analysis revealed a PilA monomer diffusion coefficient of $D_{PilA} = 0.22$ μm^2/s, which is comparable to, but slower than, the diffusion of other inner membrane proteins in

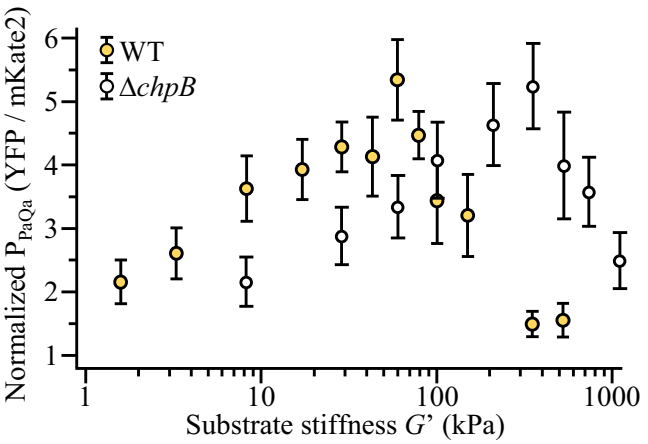

Fig. 4. The Pil-Chp system tunes the response to stiffness. The stiffness response to agarose gels of a Δ*chpB* mutant is shifted to higher stiffness compared to WT. Data points are the median of at least three biological replicates and eight technical replicates each. Error bars are the IQR of the distribution.

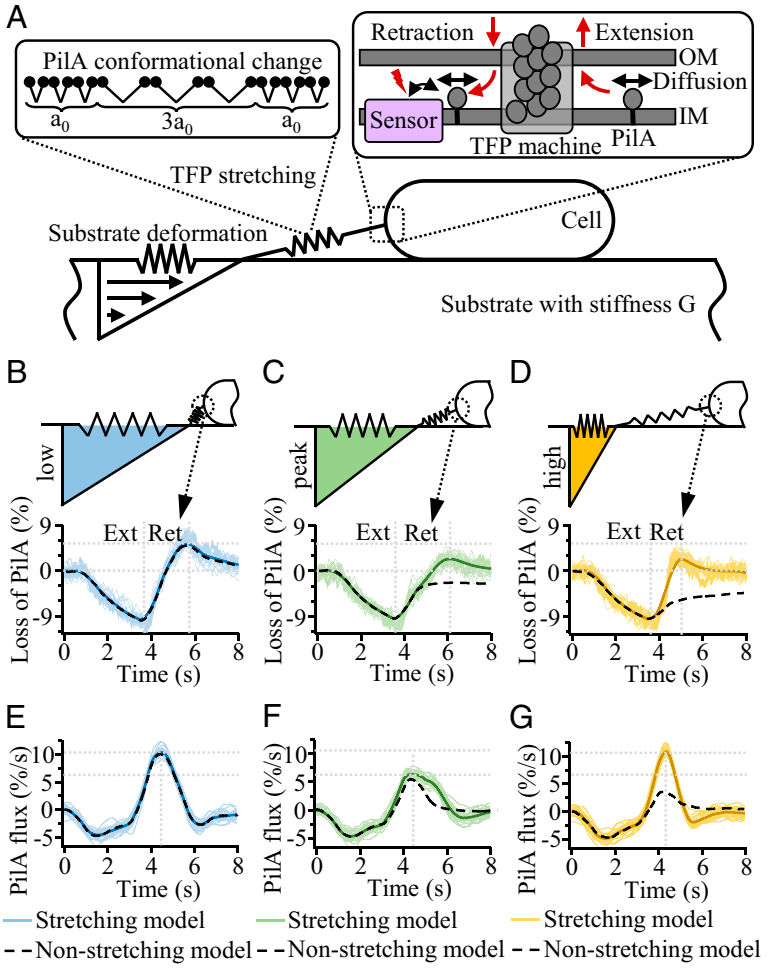

Fig. 5. Model and simulation of the TFP retraction-dependent changes in the local PilA concentration at the base of TFP on different substrates. (*A*) Sketch of the model. TFP retraction leads to elastic substrate deformation. The TFP fiber is modeled as stiff and stretching fiber, where stretching is facilitated by conformational changes of PilA (*Top left inset*). Extension and retraction result in local changes of the PilA concentration at the pole that can be sensed by a molecular PilA sensor (*Top right inset*). OM: outer membrane, IM: inner membrane. (*B–D*) The local PilA concentration at the base of TFP during TFP extension (Ext) and TFP retraction (Ret) for a gel with (*B*) low, (*C*) intermediate (at the peak of the *PaQa* response), and (*D*) high stiffness. (*E–G*) Temporal change or flux of the local PilA concentration at the base of TFP during TFP extension (Ext) and TFP retraction (Ret) for a gel with (*E*) low, (*F*) intermediate (at the peak of the *PaQa* response), and (*G*) high stiffness. (*B–G*) Black dashed lines are the median of 50 individual simulations of the nonstretching TFP model. Bold colored lines are the median of 50 individual simulations of the TFP stretching model; each individual simulation is shown as a thin colored line.

Escherichia coli (Fig. 3*G* and *SI Appendix*, *Supplementary Methods*) (41). We also found that the fluorescence intensity at the bleached pole recovered to the initial level (corrected for overall photobleaching), indicating that there is no immobile fraction of PilA monomers that are not diffusing (Fig. 3*H*).

The rate at which PilA is locally lost during TFP extension can be compared to the effect of diffusion by calculating a corresponding effective diffusion coefficient for PilA extension: A typical pilus with length $L = 1$ μm and extension velocity $v_{ext} = 350$ nm/s can be described by an effective diffusion coefficient $D_{ext} = v_{ext} \cdot L = 0.35$ μm^2/s. Even more dramatically, the pilus shown in Fig. 3*A*, with length 5 μm, yields an effective diffusion coefficient of $D_{ext} = 1.5$ μm^2/s. This shows that the loss of PilA due to extension of a pilus dominates over the diffusive behavior of PilA in the membrane in governing the concentration of PilA at the pilus base (42).

The Pil-Chp Chemotaxis System Tunes the Response to Stiffness. If changes in surface stiffness result in changes in the dynamics of the local concentrations of PilA at the base of pili, how could those PilA concentration changes be sensed in turn? Chemotaxis systems have evolved to sense rapid changes in ligand concentration, and the Pil-Chp chemotaxis-like system has previously been implicated in surface responses and cAMP induction (26, 43). Furthermore, the PilJ chemosensory receptor-like component of the Pil-Chp system has been shown to directly bind to PilA. Thus, the Pil-Chp system is an ideal candidate for translating surface-dependent changes in PilA concentration dynamics to changes in *PaQa* responsiveness. Most mutants in the Pil-Chp system eliminate *PaQa* induction altogether, making it impossible to assess the extent to which they specifically affect stiffness sensing. However, mutants in the chemotaxis adaptation systems, such as those homologous to the ChpB methylesterase from Pil-Chp, are thought to attenuate signaling without eliminating it. Consequently, we analyzed the stiffness-dependent P_{PaQa} response in a *chpB* deletion mutant. As shown in Fig. 4, this mutant is still stiffness sensitive but the P_{PaQa} response is highly attenuated, as it shifted by approximately 1 order of magnitude to a higher stiffness compared to the wild-type (WT) response (in other words, stiffer surfaces are required to induce *PaQa* in *chpB* than in WT). This result shows that the Pil-Chp system is important for stiffness sensing, and demonstrates that this system can tune the response to stiffness, which could be used as a form of signal processing to modulate stiffness sensitivity.

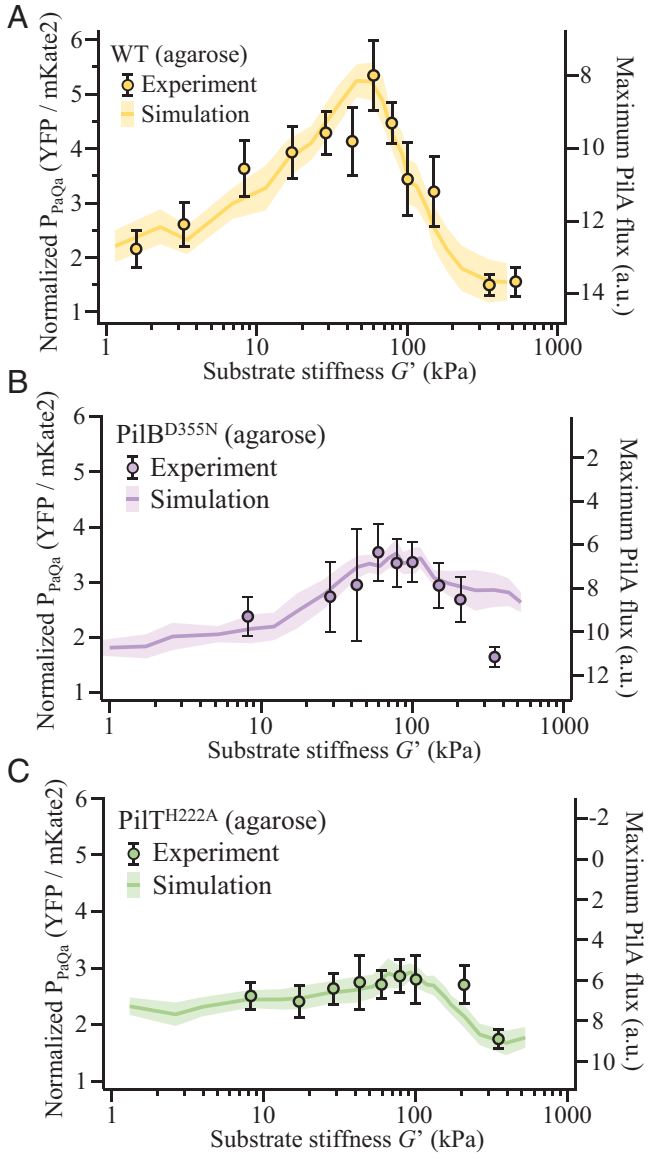

Fig. 6. Changes in the TFP extension or retraction velocity change the response to substrate stiffness in a manner that is predictive according to the model. (*A*) *P. aeruginosa* PAO1 WT cells on agarose. (*B*) The slowly extending ATPase point mutant PilB^{D355N} on agarose. (*C*) The slowly retracting ATPase point mutant PilT^{H222A} on agarose. (*A–C*) Experimental data points are the median of at least three biological replicates and eight technical replicates each. Simulations are the median of 50 individual simulations to account for the stochastic behavior of diffusion. Error bars and shading are the IQR of the distributions.

Temporal Changes of the Local Pilin Concentration Yield a Stiffness-Dependent Input Signal for a PilA Sensory System. Our results show that TFP retraction deforms hydrogel substrates, that the resulting deformation and the applied traction force depends on the stiffness of the substrate, that the concentration of PilA at the base of TFP is dynamic, and that these dynamics change with substrate stiffness. Together, these results support a model where the retraction of gel-bound TFP deforms the substrate and information about the substrate stiffness is read out by a cell via surface-dependent changes in the dynamics of the local PilA concentration at the base of TFP (Fig. 5*A*). To establish the viability of this hypothesis and help make testable predictions, we developed a quantitative model to simulate changes in PilA concentration during TFP retraction for different substrate stiffnesses.

To explain PilA levels at the pilus base, our model needed to account for the concentration change of PilA monomers driven by polymerization/depolymerization from TFP polymers and by diffusion in the membrane. To model TFP polymerization and depolymerization dynamics, we combined the experimental TFM and optical trapping results to describe the mechanical coupling of the retraction of substrate-attached TFP and the substrate deformation in a numerical simulation (*SI Appendix*, Fig. 7). In addition to the effect of force on retraction speed we measured using the optical trap (*SI Appendix*, Fig. 6), TFP also exhibited a force-induced reversible stretching under extensile loads likely due to a conformational change in the PilA monomers. This unfolding-like feature was first demonstrated in gonococcal TFP and has also been shown for TFP in *Vibrio cholerae* and *P. aeruginosa* (44–48). As shown in *SI Appendix*, Fig. 7*A*, the TFP retraction force that deforms the substrate ramps up more quickly on stiff gels compared to soft gels. Consequently, the tension in PilA monomers increases more rapidly on stiff gels. PilA thus gets stretched more quickly on stiff gels, which increases the ratio of stretched to unstretched monomers in the pilus (*SI Appendix*, Fig. 7*E*). More unstretched monomer increases the pilus rest length and thus results in more monomers that can be retracted back into the cell compared to nonstretching TFP. Focusing on the loss of PilA from the inner membrane at a fixed time point after the initiation of TFP retraction reveals a profile that is peaked with stiffness (*SI Appendix*, Fig. 7*H*). We empirically determined that a fixed time point of 0.75 s is ideal to fit the model response to the experimental P_{PaQa} data and determine optimal values for the free fit parameters (the equilibrium folding and unfolding rates of individual monomers and the attachment spot size of the TFP to the substrate).

Having accounted for PilA-level dynamics driven by TFP assembly and disassembly with a numerical mechanics simulation, we next coupled that to a simulation of stochastic PilA diffusion simulation in the inner membrane (Fig. 5*A*). This 2-tiered combined simulation is necessary to adequately describe the competition on different time scales between PilA diffusion and the TFP extension–retraction dependent change of PilA levels. As shown in Fig. 5 *B–D*, TFP extension yields a substrate–stiffness independent loss of the concentration of PilA in the inner membrane. The simulated change of PilA levels during TFP retraction on a soft gel yields an increase in the local PilA concentration above the level that was present before TFP extension started, in good agreement with our experimental observation (Fig. 5*B*, colored lines).

Having established our two-tiered model of PilA dynamics, we next examined the dependence of the system on surface stiffness. Specifically, we analyzed the temporal changes of the local PilA concentration during extension and retraction on different stiffnesses (Fig. 5 *E–G*). We found that the influx (i.e., the change in the concentration) of PilA was maximal for soft and stiff gels and lower for intermediate stiffnesses. Plotting the maximum influx of PilA during TFP retraction as a function of substrate stiffness revealed that the change in the local PilA concentration is peaked at intermediate stiffness for the stretching model and quantitatively explains the experimentally observed *PaQa* stiffness response (Fig. 6*A*). This result confirms that the dynamic changes of PilA concentration that we also observed experimentally (Fig. 3) are biophysically capable of yielding a stiffness-dependent input signal for a PilA sensory system. Interestingly, if the PilA subunits are not allowed to stretch, then the maximum influx of PilA steadily decreases with substrate stiffness and does not show a peak at intermediate stiffnesses (Fig. 4 *B–G*, black lines). Here, we modeled the

unfolding of monomers using a double-well potential function where the rate of unfolding corresponds to the Kramer's time for first barrier crossing. Although this simple description quantitatively explains the experimental results, it is possible that the unfolding of monomers is better described by a more sophisticated model, which needs to be verified by independent single-molecule stretching experiments. Together, this result suggests that stretching of PilA may be a key aspect of the mechanism that yields a peaked stiffness response.

The TFP Extension and Retraction Velocities Tune the Response to Substrate Stiffness. Our experiments and modeling suggest that *PaQa* stiffness sensing is determined by the competition between PilA diffusion and the surface stiffness–dependent outflux/influx of PilA during TFP extension–retraction. To further test this hypothesis, we investigated the effect of changes in the extension and retraction velocity on stiffness sensing. Both parameters are experimentally accessible by mutations in the ATPase activity of the PilB and PilT motors. We note that while it would also be interesting to change the diffusion of PilA in the inner membrane, this is not currently experimentally tractable.

We used two genetic mutants that separately affect the extension and retraction velocity of TFP: $PilB^{D355N}$ reduces the extension velocity on agarose from 350 nm/s to 220 nm/s (*SI Appendix*, Fig. 8), and $PilT^{H222A}$ reduces the retraction velocity from 600 nm/s to 250 nm/s (39). Using these parameters in our model predicted that both mutants should attenuate the sensitivity of stiffness sensing, with the *pilT* mutant having a stronger effect than the *pilB* mutant (Fig. 5 *B* and *C*). To test these quantitative predictions of our model, we measured the stiffness-dependent P_{PaQa} response in both $PilB^{D355N}$ and $PilT^{H222A}$ mutant backgrounds. We found that the model accurately predicted the direction and magnitude of the attenuated stiffness-sensing response in both mutants (Fig. 5 *B* and *C*). Further, we note that the difference in the location of the P_{PaQa} peak as a function of substrate stiffness between agarose and PAA gels (see Fig. 1*A*) may originate from a difference in the binding of the pilus to the gel, as predicted by our model (*SI Appendix*, Fig. 9). Together, these results demonstrate that the competition of slow PilA diffusion to fast PilA influx during TFP retraction may determine stiffness sensing and the peaked stiffness response.

Discussion

Herein, we experimentally demonstrate that the bacterium *P. aeruginosa* actively measures substrate stiffness using type IV pili and uses this information to regulate virulence-related genes in a specific stiffness range. Our experimental results suggest that the information about substrate stiffness can be encoded in temporal changes of the local PilA concentration in the inner membrane during TFP retraction. This conclusion is supported by observations that the concentration of PilA at the base of TFP is dynamic and that genetic mutations that affect the outflux or influx of PilA to/from the membrane affect stiffness sensing. A quantitative mechanical model consistently explained all these experimental observations and accurately predicted how stiffness sensing would change in mutants that affect TFP dynamics.

The dynamic range of stiffness that *P. aeruginosa* can sense covers the entire range of infection sites in the human body (22). We found that the transcriptional activity of the Vfr, which controls hundreds of virulence-related genes, is preferentially up-regulated at an intermediate stiffness range of 10 to 100 kPa (Fig. 1*B*) (49). Human tissues with stiffnesses in this range include lung, spleen, thyroid, muscle, and skin (50). This connection between pathogenesis and the mechanical properties of potential infection sites make our discovery of bacterial stiffness sensing potentially interesting for clinical application. In *P. aeruginosa*, transduction of the substrate stiffness to transcriptional activity of Vfr relies on the 2-component chemosensory system Pil-Chp. Interestingly, many clinically important pathogens like *Pseudomonas*, *Acinetobacter*, and *Stenotrophomonas* encode TFP and Pil-Chp in their genome, making this pathway and the ability to mechanically differentiate different infections sites possibly a widespread and important mechanism during the progression of bacterial infections (43).

Our results suggest that stiffness is sensed by a sensory system that is sensitive to rapid temporal changes in the dynamics of PilA concentration. The chemosensory protein PilJ of the Pil-Chp system is a prime candidate for this purpose. PilJ interacts with the major pilin PilA and is essential for *PaQa* activation (26). Furthermore, chemotaxis systems have evolved to sense temporal changes of ligand concentration, typically on the timescale of seconds (51). This time frame is consistent with the dynamics of the PilA concentration changes we observed experimentally and predicted in our model. Genetically inactivating the adaption mechanism of the Pil-Chp system tuned the response to stiffness (Fig. 4), further supporting the idea that PilJ could be sensing local PilA concentration changes to facilitate stiffness sensing. Changes in PilA levels have also been shown to stimulate the activity of the sensor kinase of the PleCD 2-component system in *C. crescentus* enabling TFP-based surface contact sensing (15, 52, 53), but whether these PilA-level changes were local or global remained unclear. Thus, our results could also help understand the mechanism by which PilA dynamics affect signaling in other systems.

Mechanotransduction allows eukaryotic cells to differentiate substrate stiffness, and this process presents a fundamental feature of embryo development and stem cell differentiation (17, 18, 54). Our experimental results and mechanical model highlight interesting parallels between stiffness sensing in eukaryotes and prokaryotes. For example, stiffness sensing by the integrin complex relies on force-dependent stretch and conformational changes that are translated into kinase activity by direct conformation-dependent ligand binding. Similarly, we show how stretch-induced conformational changes in the TFP may yield a peaked stiffness-sensitive activation of the Pil-Chp pathway and its kinase ChpA that stimulates production of the second messenger cAMP. In contrast to the direct activation in mammalian cells, we hypothesize that stiffness sensing in *P. aeruginosa* is converted indirectly from stiffness to changes in ligand concentration, which are in turn sensed by a chemotaxis system. Chemotaxis systems are widespread in bacteria, and *Pseudomonas* alone has 26 different chemoreceptors (55). These systems have evolved to sense temporal changes of ligand concentration as the small size of bacteria makes spatial sensing of ligand concentrations challenging. In contrast, the much larger mammalian cells rely almost exclusively on spatial sensing strategies. Thus, stiffness sensing may represent a conceptual parallel to chemotaxis, as in both systems large mammalian cells sense the environmental change directly while small bacterial cells use indirect changes in local concentrations to enable accurate sensing. While our results are suggestive of temporal sensing mechanism for stiffness sensing, we cannot rule out that spatial information is sensed as well (56, 57). Furthermore, stiffness sensing in mammals is typically reinforced by molecular feedback that recruits proteins to existing focal adhesions and

integrin complexes. Similarly, cAMP-dependent activation of the transcription factor Vfr yields up-regulation of TFP genes, yielding a feedback of the stiffness-sensing components.

Together, our results demonstrate that stiffness sensing is a shared ability found across both mammals and prokaryotes. Our model and genetic tests suggest that the stiffness-sensing mechanism is conceptually similar, but molecularly distinct, between both trees of life and that their specific differences have evolved to reflect their different molecular prerequisites.

Materials and Methods

Strains and Growth Conditions. Information on cloning, plasmids, and primers used in this study can be found in the *SI Appendix, Supplementary Methods* and Tables 2–4.

P. aeruginosa PAO1 was grown in liquid lysogeny broth (LB) Miller (Difco) in a floor shaker, on LB Miller agar (1.5% Bacto Agar), on Vogel-Bonner minimal medium agar (200 mg/L $MgSO_4$ 7H2O, 2 g/L citric acid, 10 g/L K_2HPO_4, 3.5 g/L $NaNH_4HPO_4$ 4 H_2O, and 1.5% agar), and on no-salt LB agar (10 g/L tryptone, 5 g/L yeast extract, and 1.5% agar) at 30 °C (for cloning) or at 37 °C. *E. coli* S17 was grown in liquid LB Miller (Difco) in a floor shaker and on LB Miller agar (1.5% Bacto Agar) at 30 °C or at 37 °C. Antibiotics were used at the following concentrations: 200 μg/mL carbenicillin in liquid (300 μg/mL on plates) or 10 μg/mL gentamycin in liquid (30 μg/mL on plates) or 10 μg/mL anhydrotetracycline in liquid for *P. aeruginosa*, and 100 μg/mL carbenicillin in liquid (100 μg/mL on plates) or 30 μg/mL gentamycin in liquid (30 μg/mL on plates) for *E. coli*.

Data Availability. All study data are included in the article and/or supporting information.

ACKNOWLEDGMENTS. We thank Ned Wingreen, Chenyi Fei, Joseph Sanfilippo, Ben Bratton, Nick Martin, Courtney Ellison, Geoff Vrla, and Benedikt Sabass for stimulating discussions and advice. We further thank our laboratory manager Joseph Sheehan and Gary Laevski from the Princeton Molecular Biology Confocal Microscopy Core Facility and the Nikon Center of Excellence. This work was supported by grants NIH DP1AI124669 and NSF MCB-2033020 (to Z.G.), NIH R21AI121828 and NSF PHY-1806501 (to J.W.S.), and Fellowship DFG KO5239/1-1 (to M.D.K.) and by the NSF through the Center for the Physics of Biological Function (PHY-1734030).

1. A. Persat *et al.*, The mechanical world of bacteria. *Cell* **161**, 988–997 (2015).
2. Z. Jiang, T. Nero, S. Mukherjee, R. Olson, J. Yan, Searching for the secret of stickiness: How biofilms adhere to surfaces. *Front. Microbiol.* **12**, 686793 (2021).
3. G. A. O'Toole, G. C. Wong, Sensational biofilms: Surface sensing in bacteria. *Curr. Opin. Microbiol.* **30**, 139–146 (2016).
4. R. Chawla, R. Gupta, T. P. Lele, P. P. Lele, A skeptic's guide to bacterial mechanosensing. *J. Mol. Biol.* **432**, 523–533 (2020).
5. K. J. Graham, L. L. Burrows, More than a feeling: Microscopy approaches to understanding surface-sensing mechanisms. *J. Bacteriol.* **203**, e00492-20 (2020).
6. G. C. L. Wong *et al.*, Roadmap on emerging concepts in the physical biology of bacterial biofilms: From surface sensing to community formation. *Phys. Biol.* **18**, 10.1088/1478-3975/abdc0e (2021).
7. B.-J. Laventie, U. Jenal, Surface sensing and adaptation in bacteria. *Annu. Rev. Microbiol.* **74**, 735–760 (2020).
8. G. N. Bruni, R. A. Weekley, B. J. T. Dodd, J. M. Kralj, Voltage-gated calcium flux mediates *Escherichia coli* mechanosensation. *Proc. Natl. Acad. Sci. U.S.A.* **114**, 9445–9450 (2017).
9. S. S. Webster, C. K. Lee, W. C. Schmidt, G. C. L. Wong, G. A. O'Toole, Interaction between the type 4 pili machinery and a diguanylate cyclase fine-tune c-di-GMP levels during early biofilm formation. *Proc. Natl. Acad. Sci. U.S.A.* **118**, e2105566118 (2021).
10. I. Hug, S. Deshpande, K. S. Sprecher, T. Pfohl, U. Jenal, Second messenger-mediated tactile response by a bacterial rotary motor. *Science* **358**, 531–534 (2017).
11. D. M. Hershey, Integrated control of surface adaptation by the bacterial flagellum. *Curr. Opin. Microbiol.* **61**, 1–7 (2021).
12. P. P. Lele, B. G. Hosu, H. C. Berg, Dynamics of mechanosensing in the bacterial flagellar motor. *Proc. Natl. Acad. Sci. U.S.A.* **110**, 11839–11844 (2013).
13. L. L. Burrows, Pseudomonas aeruginosa twitching motility: Type IV pili in action. *Annu. Rev. Microbiol.* **66**, 493–520 (2012).
14. B. Maier, G. C. L. Wong, How bacteria use type IV pili machinery on surfaces. *Trends Microbiol.* **23**, 775–788 (2015).
15. C. K. Ellison *et al.*, Obstruction of pilus retraction stimulates bacterial surface sensing. *Science* **358**, 535–538 (2017).
16. V. Vogel, M. Sheetz, Local force and geometry sensing regulate cell functions. *Nat. Rev. Mol. Cell Biol.* **7**, 265–275 (2006).
17. D. E. Discher, P. Janmey, Y. L. Wang, Tissue cells feel and respond to the stiffness of their substrate. *Science* **310**, 1139–1143 (2005).
18. A. J. Engler, S. Sen, H. L. Sweeney, D. E. Discher, Matrix elasticity directs stem cell lineage specification. *Cell* **126**, 677–689 (2006).
19. D. E. Jaalouk, J. Lammerding, Mechanotransduction gone awry. *Nat. Rev. Mol. Cell Biol.* **10**, 63–73 (2009).
20. C. C. DuFort, M. J. Paszek, V. M. Weaver, Balancing forces: Architectural control of mechanotransduction. *Nat. Rev. Mol. Cell Biol.* **12**, 308–319 (2011).
21. C. E. Harper, C. J. Hernandez, Cell biomechanics and mechanobiology in bacteria: Challenges and opportunities. *APL Bioeng.* **4**, 021501 (2020).
22. G. P. Bodey, R. Bolivar, V. Fainstein, L. Jadeja, Infections caused by Pseudomonas aeruginosa. *Rev. Infect. Dis.* **5**, 279–313 (1983).
23. G. A. O'Toole, R. Kolter, Flagellar and twitching motility are necessary for Pseudomonas aeruginosa biofilm development. *Mol. Microbiol.* **30**, 295–304 (1998).
24. A. Siryaporn, S. L. Kuchma, G. A. O'Toole, Z. Gitai, Surface attachment induces Pseudomonas aeruginosa virulence. *Proc. Natl. Acad. Sci. U.S.A.* **111**, 16860–16865 (2014).
25. B.-J. Laventie *et al.*, A surface-induced asymmetric program promotes tissue colonization by Pseudomonas aeruginosa. *Cell Host Microbe* **25**, 140–152.e6 (2019).
26. A. Persat, Y. F. Inclan, J. N. Engel, H. A. Stone, Z. Gitai, Type IV pili mechanochemically regulate virulence factors in Pseudomonas aeruginosa. *Proc. Natl. Acad. Sci. U.S.A.* **112**, 7563–7568 (2015).
27. A. K. Denisin, B. L. Pruitt, Tuning the range of polyacrylamide gel stiffness for mechanobiology applications. *ACS Appl. Mater. Interfaces* **8**, 21893–21902 (2016).
28. V. Normand, D. L. Lootens, E. Amici, K. P. Plucknett, P. Aymard, New insight into agarose gel mechanical properties. *Biomacromolecules* **1**, 730–738 (2000).
29. M. M. Chui, R. J. Phillips, M. J. McCarthy, Measurement of the porous microstructure of hydrogels by nuclear magnetic resonance. *J. Colloid Interface Sci.* **174**, 336–344 (1995).
30. D. L. Holmes, N. C. Stellwagen, Estimation of polyacrylamide gel pore size from Ferguson plots of linear DNA fragments. II. Comparison of gels with different crosslinker concentrations, added agarose and added linear polyacrylamide. *Electrophoresis* **12**, 612–619 (1991).
31. L. Jiang, S. Granick, Real-space, in situ maps of hydrogel pores. *ACS Nano* **11**, 204–212 (2017).
32. J. Narayanan, J.-Y. Xiong, X.-Y. Liu, Determination of agarose gel pore size: Absorbance measurements vis a vis other techniques. *J. Phys.: Conf. Ser.* **28**, 83 (2006).
33. J. H. Wen *et al.*, Interplay of matrix stiffness and protein tethering in stem cell differentiation. *Nat. Mater.* **13**, 979–987 (2014).
34. B. Sabass, M. D. Koch, G. Liu, H. A. Stone, J. W. Shaevitz, Force generation by groups of migrating bacteria. *Proc. Natl. Acad. Sci. U.S.A.* **114**, 7266–7271 (2017).
35. A. J. Merz, M. So, M. P. Sheetz, Pilus retraction powers bacterial twitching motility. *Nature* **407**, 98–102 (2000).
36. M. Clausen, V. Jakovljevic, L. Søgaard-Andersen, B. Maier, High-force generation is a conserved property of type IV pilus systems. *J. Bacteriol.* **191**, 4633–4638 (2009).
37. J. Ribbe, A. E. Baker, S. Euler, G. A. O'Toole, B. Maier, The role of cyclic di-GMP and exopolysaccharide in type IV pilus dynamics. *J. Bacteriol.* **199**, 00859–16 (2017).
38. C. K. Ellison *et al.*, Retraction of DNA-bound type IV competence pili initiates DNA uptake during natural transformation in Vibrio cholerae. *Nat. Microbiol.* **3**, 773–780 (2018).
39. M. D. Koch, C. Fei, N. S. Wingreen, J. W. Shaevitz, Z. Gitai, Competitive binding of independent extension and retraction motors explains the quantitative dynamics of type IV pili. *Proc. Natl. Acad. Sci. U.S.A.* **118**, e2014926118 (2021).
40. M. C. Konopka, I. A. Shkel, S. Cayley, M. T. Record, J. C. Weisshaar, Crowding and confinement effects on protein diffusion in vivo. *J. Bacteriol.* **188**, 6115–6123 (2006).
41. M. Kumar, M. S. Mommer, V. Sourjik, Mobility of cytoplasmic, membrane, and DNA-binding proteins in Escherichia coli. *Biophys. J.* **98**, 552–559 (2010).
42. S. L. Kilmury, L. L. Burrows, Type IV pilins regulate their own expression via direct intramembrane interactions with the sensor kinase PilS. *Proc. Natl. Acad. Sci. U.S.A.* **113**, 6017–6022 (2016).
43. Y. F. Inclan *et al.*, A scaffold protein connects type IV pili with the Chp chemosensory system to mediate activation of virulence signaling in Pseudomonas aeruginosa. *Mol. Microbiol.* **101**, 590–605 (2016).
44. J. L. Chlebek, T. N. Dalia, N. Biais, A. B. Dalia, Fresh extension of Vibrio cholerae competence type IV pili predisposes them for motor-independent retraction. *Appl. Environ. Microbiol.* **87**, e0047821 (2021).
45. A. Beaussart *et al.*, Nanoscale adhesion forces of Pseudomonas aeruginosa type IV pili. *ACS Nano* **8**, 10723–10733 (2014).
46. A. Touhami, M. H. Jericho, J. M. Boyd, T. J. Beveridge, Nanoscale characterization and determination of adhesion forces of Pseudomonas aeruginosa pili by using atomic force microscopy. *J. Bacteriol.* **188**, 370–377 (2006).
47. S. Lu *et al.*, Nanoscale pulling of type IV pili reveals their flexibility and adhesion to surfaces over extended lengths of the pili. *Biophys. J.* **108**, 2865–2875 (2015).
48. N. Biais, D. L. Higashi, J. Brujić, M. So, M. P. Sheetz, Force-dependent polymorphism in type IV pili reveals hidden epitopes. *Proc. Natl. Acad. Sci. U.S.A.* **107**, 11358–11363 (2010).
49. K. A. Coggan, M. C. Wolfgang, Global regulatory pathways and cross-talk control Pseudomonas aeruginosa environmental lifestyle and virulence phenotype. *Curr. Issues Mol. Biol.* **14**, 47–70 (2012).
50. C. F. Guimarães, L. Gasperini, A. P. Marques, R. L. Reis, The stiffness of living tissues and its implications for tissue engineering. *Nat. Rev. Mater.* **5**, 351–370 (2020).
51. V. Sourjik, N. S. Wingreen, Responding to chemical gradients: Bacterial chemotaxis. *Curr. Opin. Cell Biol.* **24**, 262–268 (2012).
52. L. Del Medico, D. Cerletti, P. Schächle, M. Christen, B. Christen, The type IV pilin PilA couples surface attachment and cell-cycle initiation in *Caulobacter crescentus*. *Proc. Natl. Acad. Sci. U.S.A.* **117**, 9546–9553 (2020).
53. R. A. Snyder *et al.*, Surface sensing stimulates cellular differentiation in *Caulobacter crescentus*. *Proc. Natl. Acad. Sci. U.S.A.* **117**, 17984–17991 (2020).
54. M. A. Wozniak, C. S. Chen, Mechanotransduction in development: A growing role for contractility. *Nat. Rev. Mol. Cell Biol.* **10**, 34–43 (2009).
55. D. R. Ortega *et al.*, Assigning chemoreceptors to chemosensory pathways in *Pseudomonas aeruginosa*. *Proc. Natl. Acad. Sci. U.S.A.* **114**, 12809–12814 (2017).
56. M. J. Kühn *et al.*, Mechanotaxis directs *Pseudomonas aeruginosa* twitching motility. *Proc. Natl. Acad. Sci. USA.* **118**, e2101759118 (2021).
57. N. M. Oliveira, K. R. Foster, W. M. Durham, Single-cell twitching chemotaxis in developing biofilms. *Proc. Natl. Acad. Sci. USA.* **113**, 6532–6537 (2016).